

Flux avalanches in $\text{YBa}_2\text{Cu}_3\text{O}_{7-x}$ films and rice piles: Natural time domain analysis

N. V. Sarlis,¹ P. A. Varotsos,^{1,2,*} and E. S. Skordas^{1,2}

¹*Solid State Section, Physics Department, University of Athens, Panepistimiopolis, Zografos 157 84, Athens, Greece*

²*Solid Earth Physics Institute, Physics Department, University of Athens, Panepistimiopolis, Zografos 157 84, Athens, Greece*

(Received 27 September 2005; revised manuscript received 5 December 2005; published 9 February 2006)

The measurements of the penetration of magnetic flux into a thin film of $\text{YBa}_2\text{Cu}_3\text{O}_{7-x}$ in the form of bursts or avalanches as well as those of avalanches associated with the growth of a rice pile in three dimensions are analyzed in the natural time domain χ . These two systems lead to values of the variance $\kappa_1 = \langle \chi^2 \rangle - \langle \chi \rangle^2$ and entropy $S = \langle \chi \ln \chi \rangle - \langle \chi \rangle \ln \langle \chi \rangle$ which are comparable with those obtained earlier from data analysis of other critical systems. The natural time domain analysis of a recent generalized stochastic self-organized criticality (SOC) model [A. Carbone and H.E. Stanley, *Physica A* **340**, 544 (2004)] as well as of a simple deterministic SOC numerical model [M. de Sousa Veira, *Phys. Rev. E* **61**, R6056 (2000)] is also presented and the results are compared to those of the experimental data. Both systems—i.e., $\text{YBa}_2\text{Cu}_3\text{O}_{7-x}$ and rice pile—lead to parameters κ_1 and S which distinctly differ from those deduced from a similar analysis of random telegraph signals observed in metal-oxide-semiconductor transistors with tunneling oxides.

DOI: 10.1103/PhysRevB.73.054504

PACS number(s): 74.25.Qt, 73.40.Qv, 45.70.-n, 64.60.Ht

I. INTRODUCTION

Self-organized criticality (SOC), which is a theory for large interactive systems, has been proposed^{1,2} to explain the ubiquitous occurrence of power-law behavior in nature. It states that, when large disparity exists between the time scales associated with the system driving and response, such systems will evolve naturally toward a critical state so that a minor event can lead to a major one (or catastrophe) through an avalanche process.^{1,2} The archetypal example of SOC is the growing of a sand pile. Furthermore, the critical state in superconductors has been proposed (e.g., see Ref. 3) to be a SOC system. The strong analogy between these two systems—i.e., sand piles and superconductors—as first pointed out by de Gennes (see p. 83 of Ref. 4), could be in principle understood as follows: When a type-II superconductor is put in a slowly ramped external field, magnetic vortices start to penetrate the sample from its edges. These vortices get pinned by crystallographic defects (e.g., dislocations), leading to the buildup of a flux gradient which is only marginally stable in a similar fashion as is the slope in a slowly growing sand pile. Hence, it can happen that small changes in the applied field can result in large rearrangements of flux in the sample, known as flux avalanches.⁵⁻⁷

Here in order to further investigate whether the aforementioned flux avalanches bear characteristics similar to those observed in SOC, we analyze the most recent experimental data in a new time domain (see below), termed natural time χ .⁸⁻¹³ In particular, we analyze here the flux avalanches measured¹⁴ in a thin film of $\text{YBa}_2\text{Cu}_3\text{O}_{7-x}$ (Sec. II) as well as the avalanches observed¹⁵ during the evolution of a three-dimensional pile of rice (Sec. III). Beyond the analysis of these two experimental data sets, we also analyze, in the natural time domain, the numerical results of a recent generalized stochastic SOC model¹⁶ as well as a simple deterministic SOC model^{17,18} and compare their results to those deduced from the two experimental data sets, respectively.

In a time series comprised of N events, the natural time $\chi_k = k/N$ serves as an index^{8,9} for the occurrence of the k th

event. For the analysis, we consider the evolution (χ_k, Q_k) , where Q_k stands for a quantity proportional to the energy^{8,19} of the k th event. We then define^{8,9} the continuous function $F(\omega)$, which should not be confused with the discrete Fourier transform, as follows:

$$F(\omega) = \sum_{k=1}^N Q_k \exp\left(i\omega \frac{k}{N}\right), \quad (1)$$

where $\omega = 2\pi\phi$ and ϕ stands for the natural frequency. Dividing by $F(0)$, we normalize $F(\omega)$ and obtain its power spectrum

$$\Pi(\omega) = \left| \sum_{k=1}^N p_k \exp\left(i\omega \frac{k}{N}\right) \right|^2, \quad (2)$$

where $p_k = Q_k / \sum_{n=1}^N Q_n$. For natural frequencies ϕ less than 0.5, $\Pi(\omega)$ or $\Pi(\phi)$ reduces to a characteristic function of the probability distribution p_k in the context of probability theory. As $\omega \rightarrow 0$, a Taylor expansion of Eq. (2) leads^{8,19} to $\Pi(\omega) = 1 - \kappa_1 \omega^2 + \dots$ where

$$\kappa_1 = \langle \chi^2 \rangle - \langle \chi \rangle^2 \quad (3)$$

and $\langle \chi^n \rangle = \sum_{k=1}^N p_k \chi_k^n$. It has been argued^{8,9} that for *critical* systems like seismic electric signals (SES's), (a) the variance of χ is theoretically expected to be $\kappa_1 = 7/100$ and experimentally found⁹ to be 0.070(5) and (b) the entropy S in the natural time domain (which is a dynamic^{12,20} and *not* simply statistical entropy), defined as^{8,11}

$$S = \langle \chi \ln \chi \rangle - \langle \chi \rangle \ln \langle \chi \rangle, \quad (4)$$

where $\langle \chi \ln \chi \rangle = \sum_{k=1}^N p_k \chi_k \ln \chi_k$, is smaller than the value $S_u = \ln 2/2 - 1/4 \approx 0.0966$ of a “uniform” (u) distribution. In the latter case the κ_1 value is $\kappa_1 = \kappa_u = 1/12$.

The paper is organized as follows: In Secs. II and III, we find that the data analysis in the natural time of the aforementioned two experimental data sets as well as the two numerical SOC models lead to κ_1 and S values comparable

with those expected from a critical behavior. This distinctly differs from the results obtained in Sec. IV when analyzing random telegraph signals (RTS's) observed²¹ in metal-oxide-semiconductor (MOS) transistors. This difference is discussed in Sec. IV, where we also present the interrelation between the statistical properties of SOC and the functions κ_1 and S . The main conclusions are summarized in Sec. V.

II. NATURAL TIME ANALYSIS OF FLUX AVALANCHES IN $\text{YBa}_2\text{Cu}_3\text{O}_{7-x}$ FILMS

First, we start with the observation of the penetration of magnetic flux into a thin film of $\text{YBa}_2\text{Cu}_3\text{O}_{7-x}$ by Aegerter *et al.*¹⁴ They studied the local changes in the magnetic flux over the whole central area of a sample via a highly sensitive magneto-optic setup, which allows that flux changes corresponding to $2.5\Phi_0$ can be resolved where $\Phi_0 = h/2e$ is the magnetic flux quantum (the flux of a single vortex). The pinning sites in the sample were uniformly distributed and consisted mostly of screw dislocations acting as point pins. For cuprates such as $\text{YBa}_2\text{Cu}_3\text{O}_{7-x}$ the coherence lengths are on the order of tens of Å, and thus atomic-scale structural inhomogeneities such as point defects and columnar defects can play an important role in flux-line pinning. (In these superconductors, Su *et al.*²² recently found that the Schottky-defect formation energy increases almost linearly with $B\Omega$, where B is the isothermal bulk modulus and Ω the mean volume per atom, in striking agreement with an early model suggested^{23,24} by one of the present authors.) The data of Aegerter *et al.*¹⁴ we analyze here, coming from experimental runs consisting of 140 time steps. The size and shape of the avalanches were determined from the difference $\Delta B_z(x, y)$ of two consecutive images ($50 \mu\text{T}$ increase between images), where $B_z(x, y)$ denotes the flux density at the surface of the sample measured. From these differences, the average increase in the applied magnetic field due to the stepwise field sweep was subtracted in order to solely study the avalanches. Once the incremental field difference is determined, the size of an avalanche, corresponding to the displaced amount of flux $\Delta\Phi$, is estimated from ΔB_z by integrating over the whole area $\Delta\Phi = \frac{1}{2} \int \Delta B_z(x, y) dx dy$. The time series of the avalanche behavior of a typical experiment of Aegerter *et al.*¹⁴ is depicted in Fig. 1(a), which shows that the evolution of the magnetic flux inside the sample is intermittent with occasional large jumps. In Fig. 1(b) we show the results obtained when the data of Fig. 1(a) are analyzed in natural time domain by assuming $Q_k = \Delta\Phi_k$. An inspection of the latter figure shows that for $N=140$ the κ_1 value is close to 0.070(5) and the S value is smaller than S_u . These results are compatible to those earlier deduced for the critical behavior⁸⁻¹¹ of SES's.

We now turn to the recently suggested¹⁶ model on the directed self-organized critical patterns emerging from fractional Brownian paths. This model is considered¹⁶ to be a generalized stochastic model, including the Dhar-Ramaswamy²⁵ model and the stochastic models as particular cases. In short, Carbone and Stanley¹⁶ consider a generalized Brownian walk $y(i)$ defined by $y(i) \equiv \sum_{k=0}^{i-1} \xi_k$, where the steps ξ_k are taken from a discrete Gaussian

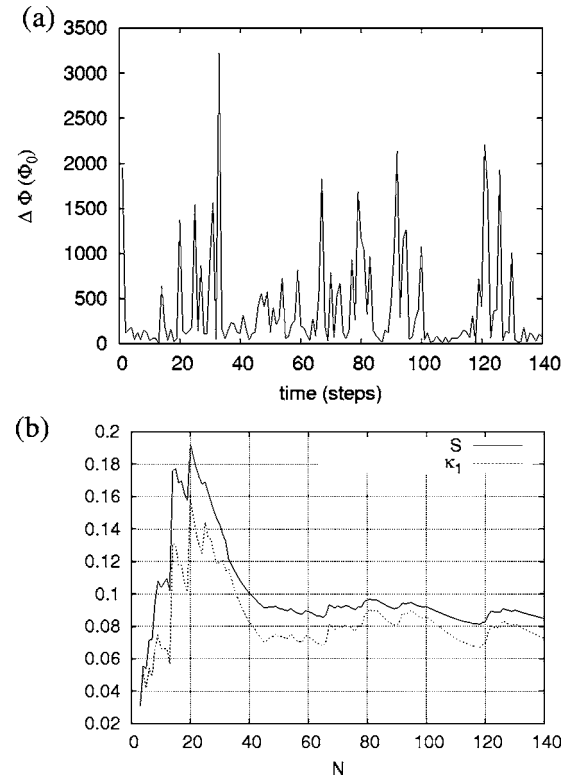


FIG. 1. (a) The time evolution of the magnetic flux in $\text{YBa}_2\text{Cu}_3\text{O}_{7-x}$ inside the sample over the first run of Fig. 2 of Ref. 14. (b) The results of the variance κ_1 (dotted line) and the entropy S (solid line) as they evolve event by event, when the data of (a) are analyzed in the natural time domain.

process with mean $\langle \xi_k \rangle = 0$ and variance $\langle \xi_k^2 \rangle = \sigma$. The mean-square displacement of $y(i)$ scales with Δi as $\langle y(i)^2 \rangle \propto (\Delta i)^{2H}$, where H is the Hurst exponent ($0 < H < 1$). The moving average function $\tilde{y}_n(i)$ is

$$\tilde{y}_n(i) \equiv \frac{1}{n} \sum_{k=0}^{n-1} y(i-k), \quad (5)$$

which is a linear operator whose output is still a generalized Brownian motion, but now with the high-frequency components of the signals averaged out according to the window amplitude n .²⁶ In order to characterize the clusters \mathcal{C} corresponding to the regions bounded by $y(i)$ and $\tilde{y}_n(i)$ in term of the characteristic exponents of SOC systems, they define—for each cluster—the cluster area s_j :

$$s_j \equiv \sum_{i=i_c(j)}^{i_c(j+1)} |y(i) - \tilde{y}_n(i)| \Delta i, \quad (6)$$

where the index j refers to each cluster. The symbols $i_c(j)$ and $i_c(j+1)$ stand¹⁶ for the values of the index i corresponding to two subsequent intersections of the “lines” defined by $\tilde{y}_n(i)$ and $y(i)$, and Δi is the elementary time interval corresponding to each step of the random walker. Then, the probability density function (PDF) $P(s)$ scales¹⁶ as $P(s) \propto s^{-\tau}$ with $\tau = 2/(1+H)$. The exponent of the avalanche distribution reported from the data analysis¹⁴ is around $\tau = 1.3$, which cor-

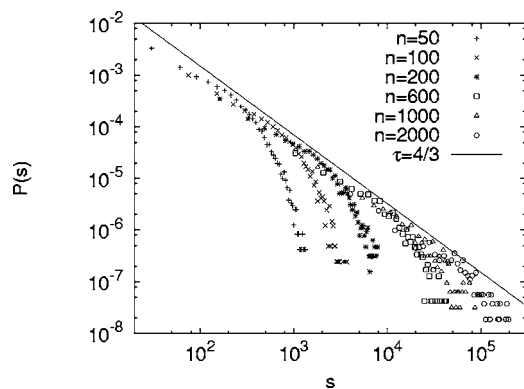


FIG. 2. The PDF $P(s)$ versus the cluster area s of the \mathcal{C} clusters of Ref. 16, for $H=0.5$ for various values of $n=50, 100, 200, 600, 1000$, and 2000 . The line $P(s) \propto s^{-\tau}$ with $\tau=4/3$, as analytically found in Ref. 16 to describe $P(s)$, is also drawn as a guide to the eye.

responds to $H \approx 0.5$. In Fig. 2, we plot $P(s)$ versus s calculated for various n values for $H=0.5$. Taking into account that the maximum avalanche size s_{max} detected by Aegerter *et al.*¹⁴ is of the order of 10^4 , an inspection of Fig. 2 leads to $n \approx 200$. In Fig. 3, we plot with solid lines the PDF's of κ_1 and S that have been obtained from the model of Ref. 16 for $H=0.5$, $n=200$, and $N=140$. The maxima of these two curves lie around $\kappa_1=0.07(1)$ and $S=0.08(1)$, respectively, which are compatible with the corresponding κ_1 and S values

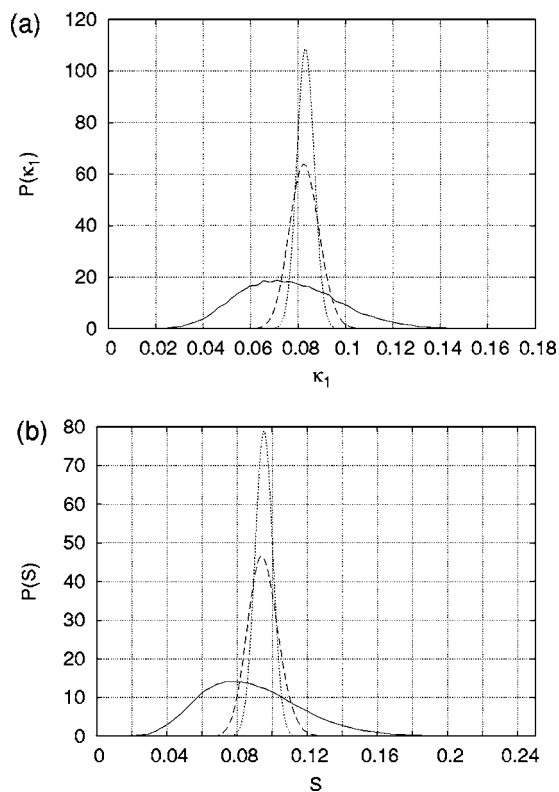


FIG. 3. The PDF's of κ_1 and S obtained from a Monte Carlo simulation for the generalized stochastic model of Ref. 16 for $H=0.5$, $n=200$, and $N=140$. The dotted and dashed PDF's correspond to two different *noncritical* cases (see the text).

depicted in Fig. 1(b) (for $N=140$). For the sake of comparison, in Fig. 3, we also plot the corresponding PDF's for two noncritical cases associated with a uniform distribution¹²—i.e., (i) when Q_k are uniformly distributed in the range $(0,1)$ (dotted line) and (ii) when Q_k are exponentially distributed (dashed line) which corresponds to a dichotomous Markovian process (see Ref. 11). The maxima of the latter two cases lie at $\kappa_1 \approx \kappa_u$ and $S \approx S_u$, which markedly differ from those deduced for $\text{YBa}_2\text{Cu}_3\text{O}_{7-x}$ in Fig. 1(b) (for $N=140$).

III. NATURAL TIME ANALYSIS OF THE AVALANCHES ASSOCIATED WITH THE GROWTH OF THREE-DIMENSIONAL RICE PILES

We now proceed to the well-controlled experiment on rice piles by Aegerter *et al.*^{15,27} Since a genuine understanding of the nature of SOC can be gained only when the *approach* to the critical state is understood, Aegerter *et al.* studied the evolution of a three-dimensional pile of rice starting well away from the critical state and getting progressively closer. The experimental results were found²⁷ to be satisfactorily described by well-founded concepts proposed²⁸ in the context of extremal dynamics. In the latter context, Paczuski *et al.*²⁸ have derived an equation (predicting power-law behavior), which they call the gap equation, describing the approach of the system to the critical state. Aegerter *et al.*¹⁵ directly studied a measure of this gap given by the maximal local slope of the rice pile and hence could test various scaling relations of extremal dynamics. Furthermore, Aegerter *et al.* studied the evolution of avalanche sizes, as well as that of the avalanche distributions, which can be used as further tests of extremal dynamics aspects. Here we focus on the way the size ΔV of the avalanches grow with time in the transient regime, which was measured directly. Figure 4(a) depicts the time evolution of ΔV obtained in one experiment of Ref. 15. In Fig. 4(b), we show the results obtained when the data of Fig. 4(a) are analyzed in the natural time domain when assuming $Q_k = \Delta V_k$. We see that actually at later times ($N \geq 350$) the κ_1 value scatters in the region around $0.07(1)$ and $S \approx 0.07(1) < S_u$, in a similar fashion as earlier found⁸⁻¹¹ for other critical systems.

We clarify that upon shuffling the data, we deduce that, for $N=550$, $\text{Prob}[\kappa_1 \leq 0.07] < 2\%$ and $\text{Prob}[S \leq 0.07] < 0.1\%$, which dictate that the *sequential order* of the avalanches captured by the natural time analysis is of prominent importance for establishing the SOC state. This could be understood in the context that in the shuffling procedure the values are put into random order, and thus all correlations (memory) are destroyed.^{11,12}

We now investigate the numerical simulations of a simple deterministic self-organized critical system introduced¹⁷ to describe avalanches in stick-slip phenomena and which is very close to the original array of connected pendulums first discussed in Ref. 1. These detailed simulations demonstrated¹⁸ that SOC itself can spontaneously generate both critical avalanche statistics and long-range temporal correlations between avalanches in the presence of a temporarily uniform, slow external drive, thus concluding that

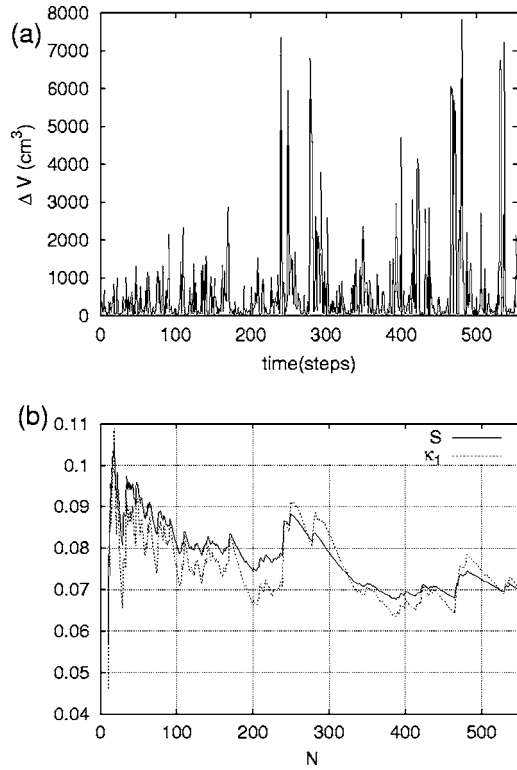


FIG. 4. (a) The evolution of the avalanche sizes, in the transient regime, for one of the experiments of Ref. 15. (b) The results of the variance κ_1 (dotted line) and the entropy S (solid line) as they evolve event by event, when the data of (a) are analyzed in the natural time domain.

SOC can be regarded as a possible mechanism for the production of $1/f^\beta$ noise. The model could be shortly defined^{17,18} as follows: Consider a one-dimensional system of size L , where a continuous (force) variable $f_\ell \geq 0$ is associated with each site ℓ . Initially all f_ℓ have the same value f_0 which is below a threshold f_{th} ; without loss of generality, one can set $f_{th}=1.0$. The basic time step consists of varying the force on the first site according to $f_1=f_{th}+\delta f$; the system then relaxes with a conservative redistribution of the force at sites $f_\ell \geq f_{th}$ (toppling sites) according to $f_\ell=\Phi(f_\ell-f_{th})$ and $f_{\ell\pm 1}=f_{\ell\pm 1}+\Delta f/2$, where Δf is the change of force at the overcritical site and $\Phi(x)$ a periodic nonlinear function. The relaxation continues until all sites have $f_\ell < f_{th}$ for all ℓ . The number of topplings, s , required for the system to relax is considered here as the appropriate value of Q_k in the natural time domain. Then, the driving force at the first site sets in again. This is complemented by open boundary conditions; i.e., the force is “lost” at $\ell=1$ and $\ell=L$. The nonlinear periodic function used here is, as in Refs. 17 and 18, a sawtooth function $\Phi(x)=1-ax+[ax]$, where $[\cdot]$ denotes the integer part of ax and a is a number. It was shown¹⁷ that such a system evolves to a SOC state where the avalanche distributions are scale free limited only by the overall system size. In this state, the total force of the system after each avalanche, $X(i)=\sum_{\ell=1}^L f_\ell(i)$, where i is the avalanche number, exhibits¹⁸ a $1/f^{1.38}$ power spectrum.

In Fig. 5, we present the results obtained from this model using $L=1024$, $a=4$, $f_0=0.87$, and $\delta f=0.1$. In Fig. 5(a) the

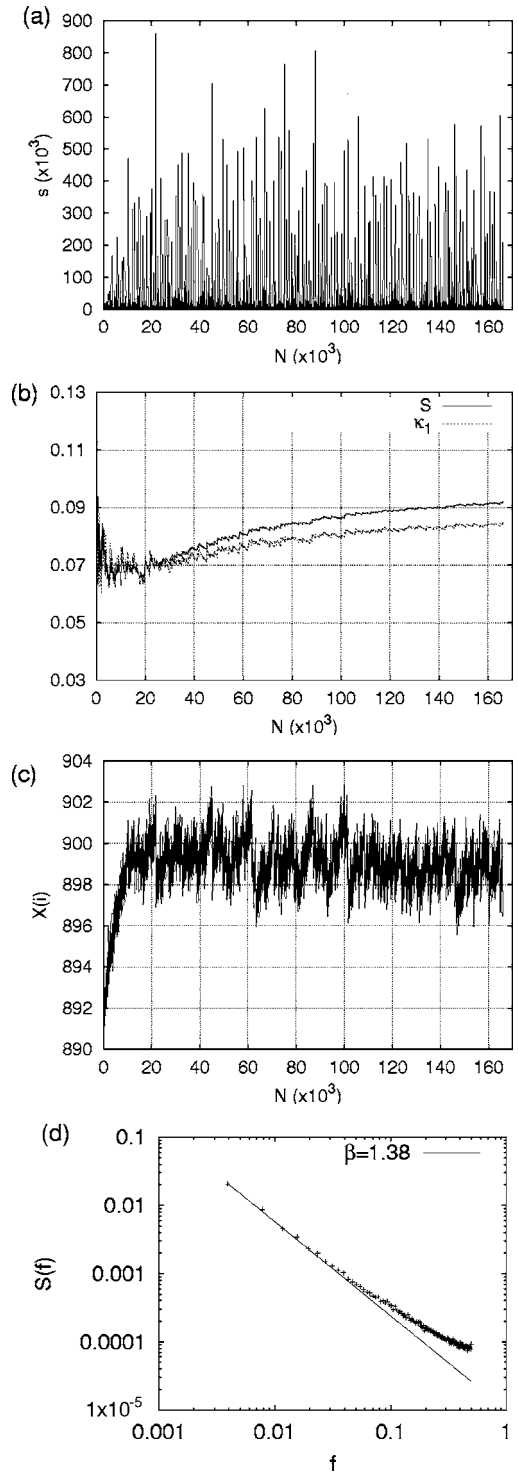


FIG. 5. (a) The results of the model studied in Ref. 18 as read in the natural time domain, $L=1024$, $a=4$, $f_0=0.87$, and $\delta f=0.1$. (b) The variance κ_1 (dotted line) and the entropy S (solid line) as they evolve avalanche by avalanche. Note that after the transient and hence when the system enters the critical state—i.e., in the region $N \in (17\,000, 30\,000)$ —we have $\kappa_1 \approx 0.07$ and $S < S_u$ (see also the relevant discussion in Sec. IV). (c) The total force of the system after each avalanche [we draw attention that after $N \geq 17\,000$ the SOC state is reached; see also (d)]. (d) The power spectrum of (c) for $N \geq 17\,000$ exhibiting the $1/f^{1.38}$ behavior as proposed in Ref. 18 for the SOC state.

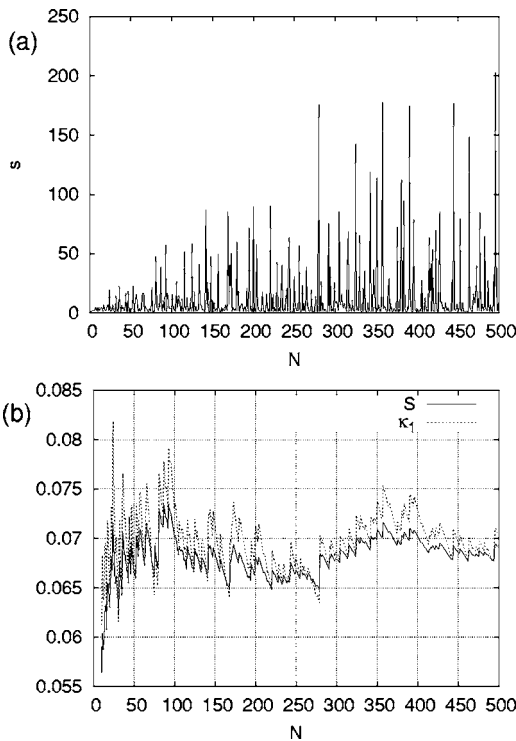


FIG. 6. (a), (b) The same as in Fig. 4, but for the avalanches calculated by the model studied in Ref. 18 using $f_0=0.5$, $\delta f=0.1$, and $a=4$.

number of topplings s is plotted versus avalanche number i ($i \equiv N$) for the first 170 000 avalanches which shows how this series of avalanches can be read in natural time. In Fig. 5(b), κ_1 and S for Fig. 5(a) are shown. In Fig. 5(c), we plot the total force $X(i)$ versus N and finally in Fig. 5(d) its power spectrum for $N \geq 17\,000$ —i.e., after the establishment of the SOC state [see Fig. 5(c)]. An inspection of Figs. 5(b) and

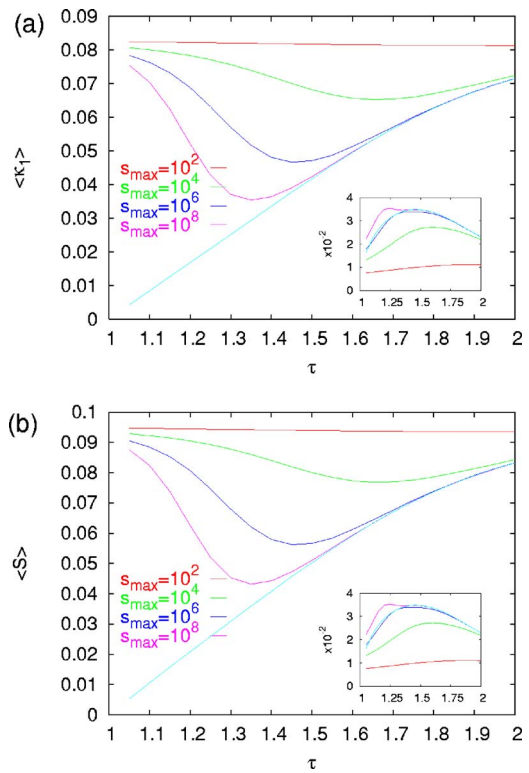


FIG. 7. (Color online) The relation between the average values of κ_1 and S and the τ exponent for various values of the maximum size of avalanche s_{max} (for $N=140$). The lowermost curve in (a) and (b) corresponds to the case $s_{max} \rightarrow \infty$. The corresponding standard deviations of the PDF's of κ_1 and S are shown in the insets, respectively.

5(c) reveals that (after the transient and hence) when the system enters into the critical state—i.e., in the range $N=17\,000$ to $\approx 30\,000$ —we have that (i) the κ_1 value be-

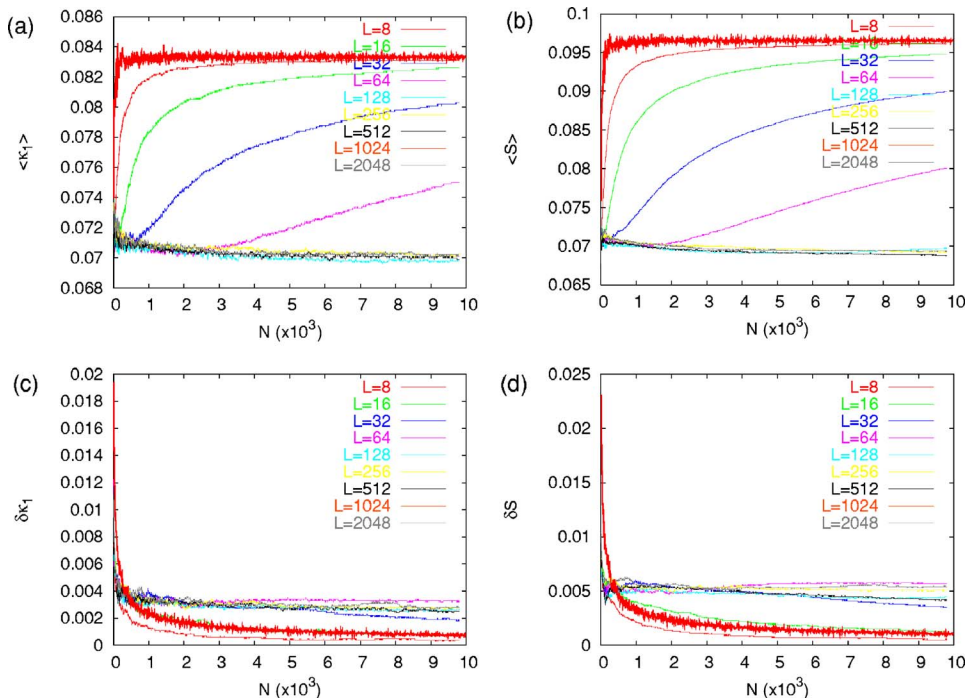


FIG. 8. (Color online) Monte Carlo simulation results for the average values and the standard deviations of κ_1 and S obtained from the model studied in Ref. 18 for $a=4$, $f_0 \in (0.25, 0.75)$, and $\delta f \in (0, 0.2)$. The corresponding results for a dichotomous Markovian process are also shown with the thick red lines.

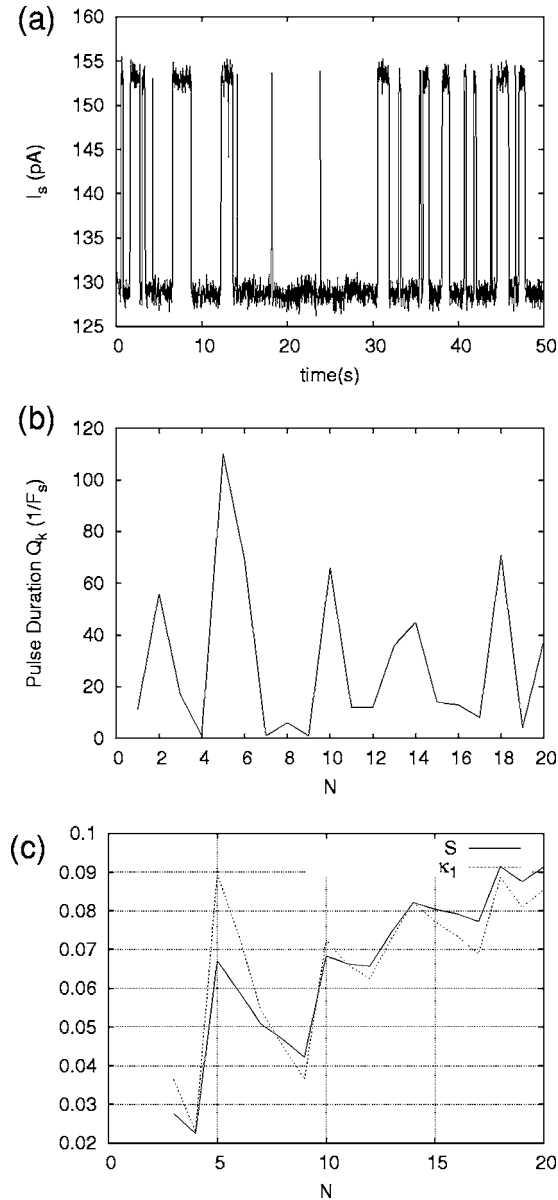


FIG. 9. (a) Example of a time record ($F_s=50$ Hz) of source currents from Ref. 21. (b) How the signal in (a) is read in natural time. (c) The results of the variance κ_1 (dotted line) and the entropy S (solid line) as they evolve event by event, when the data of (a) are analyzed in the natural time domain.

comes approximately equal to 0.070(5) and (ii) the S value is well below that of the “uniform” distribution ($S_u \approx 0.0966$), scattering approximately within the range $S=0.065$ and 0.075. This has been verified for a wide range of parameters L , f_0 , δf , and a , just before the SOC state is reached. For example, in Fig. 6 we plot for N values comparable to the experimental ones [recall that in Fig. 4(b) N is up to 550] the results of the same model in the transient stage for $f_0=0.5$, $\delta f=0.1$, and $a=4$; we then see again in Fig. 6(b) that, for $N > 350$, κ_1 and S scatter around 0.07.

IV. DISCUSSION

We first focus on a possible interrelation between the functions κ_1 and S and the statistical properties of SOC

and in particular the exponent τ . Recalling that at SOC $P(s) \propto s^{-\tau}$, a cumulative distribution function $F(s) = (1-s^{1-\tau})/(1-s_{max}^{1-\tau})$, for $\tau, s > 1$ can describe power-law-distributed avalanches up to a maximum size s_{max} . For data randomly drawn from such a distribution,²⁹ we plot in Fig. 7, for $N=140$, the average values $\langle \kappa_1 \rangle$ and $\langle S \rangle$ versus τ assuming $Q_k=s$ for various s_{max} values. In other words, this figure provides for various system sizes (and hence various s_{max}) the interrelation between the functions κ_1 and S and the exponent τ . In the case of $\text{YBa}_2\text{Cu}_3\text{O}_{7-x}$ the experimental data have $s_{max} \approx 10^4$ and $\tau=1.3$, which according to Fig. 7 correspond to $\langle \kappa_1 \rangle=0.076(1)$ and $\langle S \rangle=0.088(1)$. These values do not greatly differ from the values of κ_1 and S obtained from the analysis of the data in Fig. 1(b) (for $N=140$).

We now proceed to a system that approaches SOC as the case of rice piles in which we have seen [Fig. 5(b)] that κ_1 and S remain around 0.07 for $N > 350$. Figure 8 presents the results of a Monte Carlo simulation of the simple deterministic model of Ref. 18 for various system sizes $L=8, 16, 32, 64, 128, 256, 512, 1024$, and 2048 for the first 10^4 avalanches for $a=4$, $f_0 \in (0.25, 0.75)$ and $\delta f \in (0, 0.2)$. An inspection of this figure shows that for small system sizes—e.g., $L=8, 16$ —the values of $\langle \kappa_1 \rangle$ and $\langle S \rangle$ rapidly converge to those of a uniform distribution—i.e., κ_u and S_u , respectively. On the other hand, for large system sizes—e.g., $L \geq 128$ —the values of both κ_1 and S , after a transient ($N \leq 300$), stabilize around 0.07 even for $N \approx 10^4$ in agreement with the aforementioned behavior of the experimental data [see Fig. 4(b) for $N > 350$]. For intermediate sizes—e.g., $L=32, 64$ —the functions $\langle \kappa_1 \rangle$ and $\langle S \rangle$ initially stabilize at values ≈ 0.07 and later continuously increase towards κ_u and S_u , respectively.

Since the above systems analyzed are all *critical* systems, we now proceed for the sake of comparison to the analysis in the natural time domain of a system that exhibits substantially different behavior. We consider a case that belongs to the general case of RTS’s, which, for example, have been studied in a number of different semiconductor structures, most of all in the drain current of MOS transistors and in the gate current of MOS diodes biased in accumulation (see Ref. 30 and references therein). Here, we focus on the specific example on RTS’s measured in the low-voltage ($-1.40 < V_G < -0.88$ V) edge direct tunneling currents in ultrathin-gate-stack (10 \AA oxide + 10 \AA nitride) n -channel MOS field-effect transistors studied in Ref. 21. In this experiment, the abrupt transitions between two distinct states (i.e., the RTS phenomenon) occur in gate and source currents whereas being absent in the drain current (see Fig. 2 of Ref. 21). An example of such an RTS signal is depicted in Fig. 9(a) while in Fig. 9(b) we show how the signal in (a) is read in natural time.^{8,9} The calculated values of κ_1 and S are shown in Fig. 9(c) where it can be seen that, at $N \approx 20$, $\kappa_1 \approx 1/12$ and $S \approx S_u$, thus indicating a *random* behavior in time. (Due to the small number of events, $N \approx 20$, the results have a statistical uncertainty larger than those in the previous examples. The confidence intervals for the κ_1 and S statistics in this case can be found in Fig. 1 of Ref. 31.) This substantially differs from the behavior found in the SOC systems studied above. This can be seen in Fig. 8 in which we also include (thick red lines) the results of κ_1 and S calculated for

a dichotomous Markovian process. These show a very rapid convergence to $\kappa_1 = \kappa_{II}$ and $S = S_{II}$.

V. CONCLUSIONS

The data of the avalanches of the penetration of magnetic flux into a thin film of $\text{YBa}_2\text{Cu}_3\text{O}_{7-x}$ as well as those of a three-dimensional pile of rice getting progressively closer to the critical state when analyzed on the basis of natural time lead to values of the variance κ_1 and the entropy S which distinctly differ from those obtained from the analysis of RTS's observed in MOS transistors with tunneling oxides. The latter result in values of κ_1 and S that indicate random behavior in time, while the former (i.e., $\text{YBa}_2\text{Cu}_3\text{O}_{7-x}$ and

rice pile) are compatible with those calculated for SOC numerical models. A quantitative discussion of the relation between the functions κ_1 and S and the SOC statistical properties is put forward. Both the rice pile data and the deterministic SOC model indicate that, when approaching SOC, κ_1 becomes around 0.07(1) which has been earlier found⁹ for other critical systems.

ACKNOWLEDGMENTS

We express our sincere thanks to Dr. Rinke J. Wijngaarden for sending us the $\text{YBa}_2\text{Cu}_3\text{O}_{7-x}$ and rice pile data. We also thank Professor Ming-Jer Chen for providing us the MOS data.

*Electronic address: pvaro@otenet.gr

¹P. Bak, C. Tang, and K. Wiesenfeld, Phys. Rev. Lett. **59**, 381 (1987).

²P. Bak, C. Tang, and K. Wiesenfeld, Phys. Rev. A **38**, 364 (1988).

³S. I. Zaitsev, Physica A **189**, 411 (1992).

⁴P. G. de Gennes, *Superconductivity of Metals and Alloys* (Addison-Wesley, New York, 1989; originally published in 1966 as part of the Frontiers in Physics Series by W. A. Benjamin.).

⁵A. M. Campbell and J. E. Evetts, Adv. Phys. **50**, 1249 (2001).

⁶E. Altshuler and T. H. Johansen, Rev. Mod. Phys. **76**, 471 (2004).

⁷M. S. Welling, C. M. Aegerter, and R. J. Wijngaarden, Phys. Rev. B **71**, 104515 (2005).

⁸P. A. Varotsos, N. V. Sarlis, and E. S. Skordas, Practica Athens Acad. **76**, 294 (2001).

⁹P. A. Varotsos, N. V. Sarlis, and E. S. Skordas, Phys. Rev. E **66**, 011902 (2002).

¹⁰P. A. Varotsos, N. V. Sarlis, and E. S. Skordas, Phys. Rev. E **67**, 021109 (2003).

¹¹P. A. Varotsos, N. V. Sarlis, and E. S. Skordas, Phys. Rev. E **68**, 031106 (2003).

¹²P. A. Varotsos, N. V. Sarlis, E. S. Skordas, and M. S. Lazaridou, Phys. Rev. E **70**, 011106 (2004).

¹³P. A. Varotsos, N. V. Sarlis, E. S. Skordas, and M. S. Lazaridou, Phys. Rev. E **71**, 011110 (2005).

¹⁴C. M. Aegerter, M. S. Welling, and R. J. Wijngaarden, Europhys. Lett. **65**, 753 (2004).

¹⁵C. M. Aegerter, K. A. Lorincz, M. S. Welling, and R. J. Wijngaarden, Phys. Rev. Lett. **92**, 058702 (2004).

¹⁶A. Carbone and H. E. Stanley, Physica A **340**, 544 (2004).

¹⁷M. de Sousa Vieira, Phys. Rev. E **61**, R6056 (2000).

¹⁸J. Davidsen and M. Paczuski, Phys. Rev. E **66**, 050101(R) (2002).

¹⁹P. A. Varotsos, N. V. Sarlis, H. K. Tanaka, and E. S. Skordas, Phys. Rev. E **72**, 041103 (2005).

²⁰P. A. Varotsos, N. V. Sarlis, H. K. Tanaka, and E. S. Skordas, Phys. Rev. E **71**, 032102 (2005).

²¹M. J. Chen and M. P. Lu, Appl. Phys. Lett. **81**, 3488 (2002).

²²H. B. Su, D. O. Welch, and W. Wong-Ng, Phys. Rev. B **70**, 054517 (2004).

²³P. Varotsos, W. Ludwig, and K. Alexopoulos, Phys. Rev. B **18**, 2683 (1978).

²⁴P. Varotsos and K. Alexopoulos, *Thermodynamics of Point Defects and Their Relation with the Bulk Properties* (North-Holland, Amsterdam, 1986).

²⁵D. Dhar and R. Ramaswamy, Phys. Rev. Lett. **63**, 1659 (1989).

²⁶A. Carbone, G. Castelli, and H. E. Stanley, Phys. Rev. E **69**, 026105 (2004).

²⁷C. M. Aegerter, R. Gunther, and R. J. Wijngaarden, Phys. Rev. E **67**, 051306 (2003).

²⁸M. Paczuski, S. Maslov, and P. Bak, Phys. Rev. E **53**, 414 (1996).

²⁹R. M. Barnett *et al.*, Phys. Rev. D **54**, 1 (1996).

³⁰A. Avellán, D. Schroeder, and W. Krautchneder, J. Appl. Phys. **94**, 703 (2003).

³¹See EPAPS Document No. E-PLLEE8-68-116309 for additional information. This document can be reached via a direct link in the online article's HTML reference section or via the EPAPS homepage (<http://www.aip.org/pubservs/epaps.html>).